Biomaterials Science

ROYAL SOCIETY OF CHEMISTRY

PAPER

View Article Online
View Journal | View Issue

Cite this: *Biomater. Sci.*, 2020, **8**, 1683

Preclinical biological and physicochemical evaluation of two-photon engineered 3D biomimetic copolymer scaffolds for bone healing

Carina Kampleitner,†[a] Katayoon Changi,†[b] Reda M. Felfel,‡[c] Colin A. Scotchford,[c] Virginie Sottile,[d] Rainer Kluger,[e] Oskar Hoffmann,[a] David M. Grant[c] and Michelle M. Epstein *[b]

A major challenge in orthopedics is the repair of large non-union bone fractures. A promising therapy for this indication is the use of biodegradable bioinspired biomaterials that stabilize the fracture site, relieve pain and initiate bone formation and healing. This study uses a multidisciplinary evaluation strategy to assess immunogenicity, allergenicity, bone responses and physicochemical properties of a novel biomaterial scaffold. Two-photon stereolithography generated personalized custom-built scaffolds with a repeating 3D structure of Schwarz Primitive minimal surface unit cell with a specific pore size of ~400 μm from three different methacrylated poly(D,L-lactide-*co*-ε-caprolactone) copolymers with lactide to caprolactone monomer ratios of 16 : 4, 18 : 2 and 9 : 1. Using *in vitro* and *in vivo* assays for bone responses, immunological reactions and degradation dynamics, we found that copolymer composition influenced the scaffold physicochemical and biological properties. The scaffolds with the fastest degradation rate correlated with adverse cellular effects and mechanical stiffness correlated with *in vitro* osteoblast mineralization. The physicochemical properties also correlated with *in vivo* bone healing and immune responses. Overall these observations provide compelling support for these scaffolds for bone repair and illustrate the effectiveness of a promising multidisciplinary strategy with great potential for the preclinical evaluation of biomaterials.

Received 12th November 2019,
Accepted 17th January 2020

DOI: 10.1039/c9bm01827a

rsc.li/biomaterials-science

Introduction

The repair of large non-union bone lesions may be a major complication of traumatic injury, metabolic bone disease like osteoporosis and tumours.[1,2] The development of synthetic biomaterials to fill bone defects and accelerate bone healing is a growing field,[1,3] because autologous, allogeneic and cadaver bone grafts, which are the gold standard for bone repair, are associated with a myriad of complications and limited availability.[1,2,4,5] Bone substitutes or synthetic grafts can overcome the limitations of autologous and allogeneic bone grafts.[3] A large range of osteoconductive and osteoinductive biomaterials for bone repair are promising[2] including bioengineered biodegradable materials that provide structure within the bone lesion while being replaced by newly formed bone during bone regeneration.

The biology of bone fracture healing is a multistage process that follows a specific cascade resulting in unscarred restoration of bone tissue.[6] Local and systemic growth and differentiation factors, hormones, cytokines and extracellular matrix proteins interact with cells in the circulation and fracture site[7] and begin with an inflammatory phase, followed by repair and bone remodeling.[8] Transient inflammation after injury is essential[6,9,10] to produce factors that initiate osteoblast (OB)- and osteoclast (OC)-mediated bone repair. Bone biomaterials should not induce chronic inflammation or fibrosis but should promote mild inflammation, followed by osteoconduction or induction, provide mechanical support and degrade over time.[11] If biomaterials induce excessive inflammation and/or immune and allergic responses, inhibition or delay of bone repair may occur.[12,13]

[a]*Department of Pharmacology and Toxicology, University of Vienna, Vienna, Austria*
[b]*Laboratory of Experimental Allergy, Division of Immunology, Allergy and Infectious Diseases, Medical University of Vienna, Department of Dermatology, Vienna, Austria. E-mail: Michelle.Epstein@meduniwien.ac.at; Fax: +431 40160 963012; Tel: +431 40160 63012*
[c]*Advanced Materials Research Group, Faculty of Engineering, University of Nottingham, UK*
[d]*Danube Hospital Vienna, Vienna, Austria*
[e]*Wolfson STEM Centre, School of Medicine, University of Nottingham, UK*
†These authors contributed equally.
‡Present address: R.A. Felfel is an associate professor at the Physics Department, Faculty of Science, Mansoura University, Egypt.

A porous three-dimensional (3D) scaffold for bone repair ideally should mimic an autologous bone graft,[14] be biodegradable and either induce minimal inflammation or no inflammation, in combination with the factors that promote bone repair and should not cause fibrosis or scarring.[15] Examples of biodegradable polymers that are resorbed overtime frequently used in regenerative medicine[16–18] include polyglycolic acid (PGA), polylactide (PLA), polylactic-*co*-glycolic acid (PLGA), poly-ε-caprolactone (PCL), poly(D,L-lactide) (PDLLA) and additional copolymers and composites.[19,20] Although scaffold degradation is beneficial, undesired effects caused by degradation products *via* the formation of small chain carboxylic acids may change the local pH and cause inflammation[21,22] or in some cases as occurs within PLA, acidic degradation products may be toxic.[17] Methods developed for the production of these porous polymeric materials include electrospinning, phase separation and porogen leaching. However, these techniques do not enable the manufacture of complex 3D structures with tunable micro-scale features.

Computer-aided design (CAD) based technologies like 3D-printing and stereolithography are capable of manufacturing scaffolds for tissue engineering, but to obtain true biomimetic or well-defined structures, sufficient resolution is required.[23] Two-photon polymerization (TPP) is an example of stereolithography technology, which is capable of fabricating well-defined 3D microstructures with a resolution of 100 nm.[24,25] For bone filling scaffolds, the optimum pore size ranges from 200 to 400 μm, which is similar to the average size of a human osteon (~223 μm).[26] Moreover, it is possible to design and produce customizable scaffolds that are compressible and tailored to fit into the fracture site. One limitation in the past for TPP has been the slow scan speeds but as the technology improves exciting capability is now available to deliver high-resolution scaffolds in commercially attractive timescales.

In this study, we used methacrylated poly(D,L-lactide-*co*-ε-caprolactone) (PLCL) copolymers of different compositions and chain lengths (LCM3 (16 : 4), LCM4 (18 : 2) and LCM6.1 (9 : 1)). These numbers represent the monomer units of lactide (LA) and caprolactone (CL) used to generate biomimetic 3D Schwarz Primitive (P) minimal surface scaffold structures with a pore size of 400 μm.[27,28] Here, we combine materials science, bone biology and immunology to establish a strategy for evaluating these developed TPP-engineered copolymer scaffolds for eventual use in patients. The biomaterials were assessed using three approaches: (1) an *in vitro* evaluation of osteoblast and osteoclast function and an *in vivo* mouse calvarial defect model to assess bone healing in the context of the scaffolds, (2) *in vitro* degradation and mechanical studies (compressive strength and modulus), and (3) *in vitro* and *in vivo* evaluation of inflammatory, immune and allergic reactions. The *in vitro* assay provides information on antigen cross-reactivity and cytotoxicity; the rapid high-throughput intraperitoneal assay provides data on the inflammation and the cytokine milieu; and the sub-chronic subcutaneous long-term assay provides information on the longevity of the inflammatory response and the capacity of the biomaterial to induce fibrosis.

Materials and methods

Ethics statement

This study was carried out in strict accordance with the guidelines for the Care and Use of Laboratory Animals of the Austrian Ministry of Science. The protocol was approved by the Committee on the Ethics of the Austrian Ministry of Science (No: 66:006/00 12-11/3b/2012). All painful procedures were performed under anesthesia, and all efforts were made to minimize suffering.

Mice

Female 8–12 week old BALB/c and C57BL/6 (B6) mice (Charles River Laboratories, Sulzfeld, Germany) were used for *in vivo* experiments. Neonatal mice were used for the isolation of OBs. The mice were housed in the mouse facility at the Department of Pharmacology and Toxicology, University of Vienna, Vienna, Austria. Mice were provided food (Ssniff Spezialdiäten GmbH, Soest, Germany) and tap water *ad libitum*.

2D copolymer disk and 3D scaffold production

LCM scaffolds were produced and provided by the Institute for Bioprocessing and Analytical Measurement Techniques (iba, Heiligenstadt, Germany) and the detailed description of the methodology can be found in ref. 27. Briefly, methacrylated PLCL copolymers were synthesized by ring opening polymerization. Three different LA/CL ratios were used and coded LCM3 (16 : 4), LCM4 (18 : 2) and LCM6.1 (9 : 1). Both LCM4 and LCM6.1 have the same molar ratio (LA/CL) of 18 : 2 and 9 : 1 respectively compared to LCM3 which is 16 : 4. However, LCM6.1 has lower molecular weight (1059 g mol^{-1}) than LCM4 (1822 g mol^{-1}) and LCM3 (1742 g mol^{-1}).[29]

For disk manufacturing, precursor-LCMs and photoinitiator (Irgacure369 (0.1 wt%), BA740 (0.2 wt%)) were filled into a silicon mold (∅ = 5 mm, 0.5 mm height) and solidified by 9 min of UV irradiation (Vacuum-UV-Exposure Box2, proMa). The polymer disks were developed in acetone for 7 days before drying under vacuum and sterilized using gamma irradiation at the dose of 25 ± 2.5 kGy and kept in sterilization pouches prior to use. For 3D scaffold manufacturing, photoinitiator and LCM precursors underwent polymerization with a TPP apparatus (M3DL, LZH Hannover, Germany) with a femtosecond laser source (140 fs, 80 MHz, 800 nm) to produce LCM scaffolds followed by washing in acetone to remove the unpolymerized precursors. The produced repeating array of Schwarz P unit cell (with 400 μm size) scaffolds were sterilized using gamma irradiation as described above (Table 1).

In vitro bone cultures

Osteoclasts. To study effects on osteoclastogenesis, we performed a co-culture model using primary mouse OBs and bone marrow OC precursors as previously described.[30] Primary

Table 1 Structural properties of the produced LCM scaffolds

Scaffold type	Pore size (μm)	Throat size (μm)	Wet weight change (%) after ~12 weeks *in vitro* (in PBS at 37 °C)
LCM3	314 ± 14	177 ± 7	214
LCM4	328 ± 26	177 ± 10	252
LCM6.1	290 ± 25	152 ± 7	121[a]

NB. Previously published;[29] shows percentage weight change of scaffolds as wet at the end of *in vitro* degradation. [a] Wet weight change of LCM6.1 scaffold was recorded after 69 days.

mouse OBs were isolated from neonatal mouse calvarial bones using enzymatic digestion.[31] These OBs (6.2×10^4 cells per cm^2) were cultured together with bone marrow OC precursors harvested from mouse femurs and tibiae in αMEM (Gibco, Thermo Fisher Scientific, Vienna, Austria), 10% heat-inactivated fetal bovine serum (FBS, Gibco), 1% penicillin/streptomycin (Gibco), 1 nM 1,25-$(OH)_2$-vitamin D_3 (Sigma-Aldrich, Vienna, Austria) and 1 μM prostaglandin E2 (PGE_2, Cayman Chemicals, Hamburg, Germany) onto 96-well culture plates containing the copolymer disks (∅ = 5 mm) or onto tissue culture plastic at 37 °C and 5% CO_2. At day 6 of co-culture, histochemical staining for tartrate-resistant acid phosphatase (TRAP) was done to characterize OCs. Cells were fixed in 3.7% buffered formaldehyde (Carl Roth, Vienna, Austria) at RT and stained with 1 mg ml^{-1} naphthol AS-MX phosphate (Sigma-Aldrich), 0.6 mg ml^{-1} fast red violet salt (Sigma-Aldrich) and 10 mM sodium tartrate (Sigma-Aldrich). TRAP+ multinucleated cells (TRAP+ MNCs) with 3 or more nuclei were considered mature OCs and enumerated under a light microscope (Nikon Diaphot 300, Japan).

Osteoblasts. Primary mouse OBs (6.2×10^4 cells per cm^2) were seeded in αMEM, 10% FBS and 1% penicillin/streptomycin onto 96-well culture plates containing the 2D copolymer disks (∅ = 5 mm) or onto tissue culture plastic at 37 °C and 5% CO_2. To induce OB differentiation, culture medium was supplemented with 50 μg ml^{-1} ascorbic acid (Sigma-Aldrich) and 5 mM β-glycerophosphate (Sigma-Aldrich) 24 h post seeding. OBs cultured in medium alone served as the control group. OB cell proliferation was evaluated by "Presto Blue cell viability assay" (Molecular Probes, Thermo Fisher Scientific, MAN0003232) according to the manufacturer's instructions. Briefly, cells were incubated with Presto Blue reagent and the reagent was reduced by metabolically active cells. This serves as an indicator for cell viability and proliferation. The reduction product was detected at 560/590 nm. At day 7, alkaline phosphatase (ALP) activity was measured as a marker for OB differentiation from cell lysates with a fluorogenic substrate (6,8-difluoro-4-methylumbelliferyl phosphate, DIFMUP, Molecular Probes, Thermo Fisher Scientific) at 388/455 nm as previously described.[32] ALP activity was also detected using SIGMAFAST™ BCIP®/NBT substrate stain (Sigma-Aldrich) according to the application note of PromoCell (Heidelberg, Germany). Calcium deposition of mature OBs was visualized by Alizarin Red S (ARS) and von Kossa staining at day 14. For ARS staining, cells were fixed in 10% neutral buffered formalin (Sigma-Aldrich) and stained with 40 mM ARS (pH 4.2) (Sigma-Aldrich). Quantification of ARS-stained cultures was performed by a cetylpyridinium chloride extraction method and extracts were read at 520 nm. For von Kossa staining, cells were fixed in 10% neutral buffered formalin (Sigma-Aldrich) and incubated with 5% silver nitrate solution (Sigma-Aldrich) under UV light before neutralization with 5% sodium thiosulfate (Sigma-Aldrich). All stained plates were scanned on a high-resolution flat-bed scanner (Epson Perfection 1200Photo, Vienna, Austria).

In vivo intracalvarial defect model

The LCM scaffolds (∅ = 4 mm) were incubated overnight in sterile PBS. Orthovita Vitoss™ Foam (Vitoss, Malvern, USA) was used in the experiments as a positive control. Vitoss was cut into 4 mm diameter and then soaked in 50 μl PBS before implantation. Non-healing critical, full-thickness size defects were created in anesthetized (100 mg kg^{-1} ketamine (Ketamidor®, Richter Pharma, Wels, Austria) and 5 mg kg^{-1} xylazine (Rompun®, Richter Pharma)) 12-week old female BALB/c mice (n = 5–6) in the right parietal bone using a dental trephine with 4 mm diameter under constant irrigation while preserving the underlying dura mater. LCM scaffolds or Vitoss were implanted into the defect or left empty and then the skin was sutured. The animals were monitored post-op and treated with 0.1 mg kg^{-1} buprenorphine (Bupaq®, Richter Pharma) for analgesia every 10–12 h for 3 days. At 12 weeks post-operation, the animals were sacrificed by cervical dislocation, and skulls were harvested and fixed in 4.5% buffered formalin (Carl Roth). For histological examination, light-curing resin (Technovit 7200 VLC + 1% benzoyl peroxide, Heraeus Kulzer, Wehrheim, Germany) embedded undecalcified sections (80–100 μm) were prepared parallel to the sagittal suture with an Exakt Cutting and Grinding Equipment (Exakt, Norderstedt, Germany) and stained with Levai Laczko dye according to a standardized method.[22]

Immunological assessment

***In vivo* immunological assessment of scaffolds.** The LCM scaffolds (2 mm^3) were incubated overnight in sterile PBS. Vitoss was used in all immunological experiments as a positive control because it contains type I bovine collagen, which is recognized as a foreign protein and generates an immune response in mice. Vitoss was cut into 2 mm^3 and then soaked in 50 μl PBS before implantation. Scaffolds and Vitoss were implanted either intraperitoneal (i.p.) or subcutaneous (s.c.) into 8-week old female BALB/c and B6 mice (n = 5) and compared to age-matched sham controls. For implantation, mice were anesthetized with 100 mg kg^{-1} ketamine (Ketanest®, Pfizer Corporation Austria GmbH., Vienna, Austria) and 6 mg kg^{-1} xylazine (Rompun®, Bayer AG, Leverkusen, Germany).

For the high throughput model, we used the implantation approach described in ref. 33 and 34. Abdominal fur was shaved and cleaned with 70% alcohol and polyvidone iodine (Betadine®). An 8 mm midline incision was made aseptically

along the linea alba followed by an incision in the peritoneum. LCM scaffolds or Vitoss were placed in the peritoneal cavity. The abdominal muscles and skin were sutured with absorbable 4-0 Vicryl suture (Ethicon Inc., Somerville, USA) and 4-0 nylon suture (Ethicon), respectively. The same incision and suture were used without implanting materials for the sham controls. The peritoneal cavity was lavaged 7 days after implantation with 3 ml PBS and peritoneal cells were counted and peritoneal fluid was stored at −20 °C until thawed for the measurement of IL-1β (eBioscience Inc., San Diego, USA), IL-2 and IL-4 (ELISA MAX™ Standard, Biolegend, San Diego, USA) cytokines.

For the subchronic model, we used the implantation approach described in ref. 33 and 35. An 8 mm midline abdominal incision of the skin along the linea alba was made under aseptic conditions. LCM scaffold or Vitoss of the same size (2 mm^3) or no materials were inserted s.c. and then the skin was closed with 4-0 nylon suture. The mice were monitored until recovery from anesthesia. At 12 weeks, the implantation site with surrounding tissue (10 mm^2) from each mouse was excised and fixed in 4% formaldehyde overnight and then embedded in paraffin. Tissue sections (4 μm) were prepared and stained with Hematoxylin and Eosin (H&E) and Masson's trichrome (Sigma-Aldrich).

***In vitro* splenocyte responses to scaffolds.** LCM copolymer disks (∅ = 5 mm) were incubated with BALB/c and B6 mouse splenocytes. Spleens were minced and passed through a sterile 40 μm cell strainer (Corning Life Sciences, Durham, USA) in cold, sterile PBS. The cells were centrifuged and RBCs were lysed with lysis buffer (BD Pharm Lyse™, BD Bioscience, New Jersey, USA). Titrated numbers of splenocytes were suspended in RPMI with 10% FBS, 1% penicillin/streptomycin, 0.1% gentamicin (Gibco), 0.2% β-mercaptoethanol 50 mM (Gibco) and 1% (100×) non-essential amino acids (Gibco) and were incubated with the copolymer disks, Vitoss, 10 μg ml^{-1} Concanavalin A (ConA, Amersham Pharmacia Biotech, Piscataway, USA) or a combination of ConA and biomaterials in a 96-well plate at 37 °C at 5% CO_2 for 72 h. Cell proliferation was measured using a cell proliferation ELISA BrdU kit (Roche Diagnostics, Vienna, Austria) by adding BrdU at 48 h and measuring absorbance at 450 nm at 72 h. In addition, supernatants were removed at 72 h and stored at −20 °C until thawed for the ELISA measurements of IL-1β, IL-2, IL-4 and IFNγ (ELISA MAX™ Standard, Biolegend, San Diego, USA).

Scaffold degradation studies

The degradation study was performed for LCM scaffolds of dimensions 2 mm^3 according to the standard BS EN ISO 10993-13:2010.[36] The high reproducibility of the method due to the TPP production allows individual scaffolds to be followed through their degradation pathway.[27] Scaffolds were placed individually into glass vials containing 30 ml PBS (pH = 7.4 ± 0.2) solution and maintained in an oven at 37 °C. At various time points, the specimens were extracted with tweezers, placed into empty vials and dried in a vacuum oven (Medline Scientific, UK) at 50 °C for 60 min. Afterwards, the dry weight of the scaffolds was recorded, and samples were then returned to vials containing fresh PBS. The percentage mass loss (M_L) at each time point was calculated using the following equation;

$$M_L = \left(\frac{m_d - m_i}{m_i}\right) \times 100(\%)$$

where m_d is the mass of the degraded scaffold after drying at 50 °C in the vacuum oven for 60 min and m_i is the initial dry mass of the scaffold.

Optical images of dried LCM scaffolds were captured at each degradation time point using a Nikon digital camera (Dxm1200F, Japan) attached to Nikon microscope (Japan). The images were processed using image analysis software (Nikon ACT-1 v. 2.62, LEAD Technologies, USA).

Mechanical test

The compressive strength and modulus were determined using Hounsfield tester, and the calculations were done according to the standard ASTM 1621-10:2010.[37] Scaffolds were inserted vertically between two flat plates of the testing machine where the load was applied on the cross-section of the scaffold. A crosshead speed of 0.5 mm min^{-1} and a 5 N load cell was used, and the test was carried out up to 20% strain (below the yield strain of the specimens) to prevent permanent deformation within the scaffolds. At various time points, the specimens were removed from PBS and dried in a vacuum oven at 50 °C for 60 min before testing. The measurements were applied on dry scaffolds and carried out in three successive cycles with a time interval of 10 min to permit scaffold recovery. The compressive strength is taken as the maximum stress at 20% strain, while compressive modulus was determined as the gradient of the linear portion of stress–strain curve. The samples were then placed back in the medium until the next time point.

Statistical analysis

Statistical analysis of biological assays was done using one-way analysis of variance (ANOVA) with Tukey's *post hoc* test for multiple comparisons (GraphPad Prism v 5.0, San Diego, USA). p values were considered significant at <0.05.

Results

In vitro assessment of OC and OB differentiation and maturation

To determine the effect of scaffolds on OC differentiation, OBs and bone marrow OC precursors were co-cultured in the presence of LCM3, 4 and 6.1 scaffolds and the medium alone (M) control group (Fig. 1A). The OC morphology differed between the M control and LCM3, 4 and 6.1 scaffolds with a high number of differentiated mature multinucleated TRAP+ OCs (≥3 nuclei) in the M controls. In contrast, the LCM scaffolds induced fewer, smaller and less spread out, irregularly-shaped mature OCs. TRAP+ multinucleated OCs for the M group were

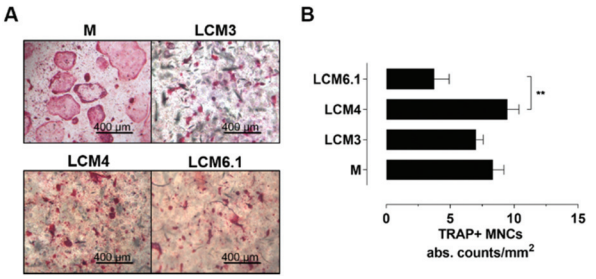

Fig. 1 Scaffold-induced *in vitro* OC differentiation and maturation. Mouse OC differentiation was determined at day 6 of co-culturing mouse OBs and bone marrow OC precursors in the presence of 1,25-$(OH)_2$-vitamin D3 and PGE_2. (A) Representative images show TRAP+ MNCs for medium (M) control group, LCM3, 4 and 6.1. (B) Endpoint analysis of TRAP+ MNCs. The graph shows the absolute count of TRAP+ MNCs (≥3 nuclei) per mm^2 (mean ± SEM, n = 6). **p < 0.01.

$8.34 \pm 0.87\ mm^{-2}$ and for the scaffolds were LCM3: $7.01 \pm 1.39\ mm^{-2}$, LCM4: $9.47 \pm 0.90\ mm^{-2}$ and LCM6.1: $3.74 \pm 1.17\ mm^{-2}$ (Fig. 1B). LCM3 and M controls induced a similar number of differentiated TRAP+ OCs compared to LCM4, though only LCM4 was statistically significantly higher compared to LCM6.1 ($p < 0.01$). These data demonstrate that LCM6.1 significantly reduced OC differentiation compared to the other tested groups.

To determine the effect of LCMs on OBs, the OB viability and proliferation was evaluated using the Presto Blue assay. The OB proliferation peaked at day 3 in the presence of the scaffolds (Fig. 2A) and was significantly higher for LCM3, 4 and 6.1 compared with osteogenic medium (OM) controls. The OB proliferation increased minimally and remained stable for the OM controls over the 14-day culture period. In contrast, LCM3 induced proliferation from day 1 to day 3 that remained stable until day 14, whereas LCM4 and LCM6.1 increased proliferation initially followed by decreased proliferation after day 7 with a more prominent reduction for LCM6.1. These data demonstrate that there were more proliferating OBs in the presence of LCM3 compared with LCM4 and LCM6.1.

To analyze OB differentiation, cells (Fig. 2B) were stained, and the ALP activity was measured (Fig. 2C). The OBs differentiated normally into more mature OBs and had higher ALP activity in the OM compared to M control alone (Fig. 2B and C). In Fig. 2B, the number of stained ALP+ cells was increased in all groups compared to controls without mineralization medium. However, the staining pattern exhibited when the cells were on LCM disks differed from the OM controls. Nevertheless, when we quantified the ALP activity in OBs, no statistical difference in ALP activity between OM and LCM groups was observed.

To assess OB mineralization, cultured OBs were stained with ARS and von Kossa. LCM6.1 and LCM4 induced higher mineralization compared with LCM3 and OM samples as shown in the tissue culture plate wells (Fig. 2D) and by absorbance of the extracted ARS calcium complex measurements (Fig. 2E). These data show that LCM4 and LCM6.1 disks supported higher matrix mineralization than LCM3.

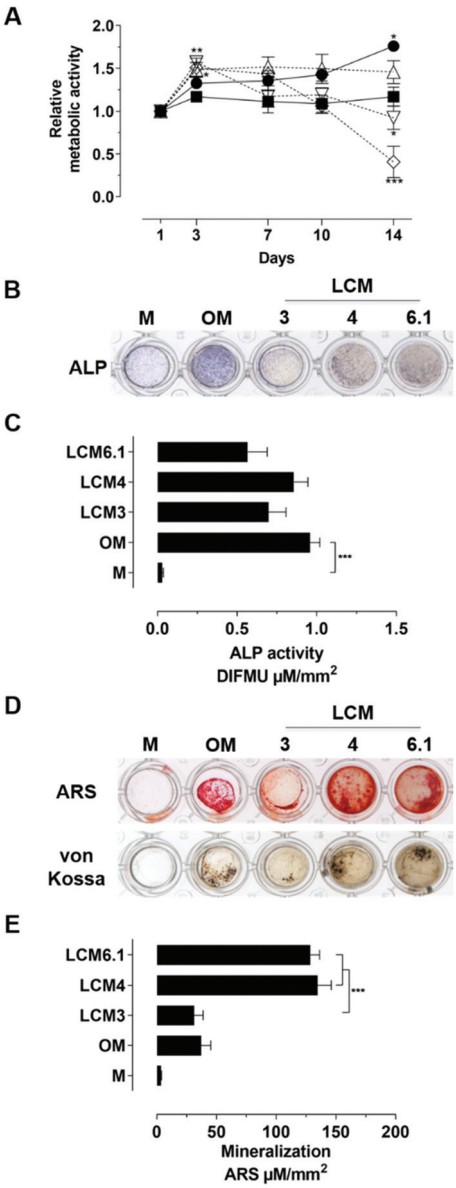

Fig. 2 Scaffold-induced *in vitro* OB differentiation and maturation. (A) OB proliferation was determined on days 1, 3, 7, 10 and 14 by Presto Blue assay upon incubation with either medium alone (M) ●, osteogenic medium (OM) ■, LCM3 △, LCM4 ▽ and LCM6.1 ◊ illustrated by relative metabolic activity. Relative metabolic activity is demonstrated as fold increase or decrease calculated from fluorescence units and normalized to day 1 within each group (mean ± SEM; n = 4–6). Day 3: LCM3 and 6.1 *vs.* OM *p < 0.05, LCM4 *vs.* OM **p < 0.01, day 1: M *vs.* OM *p < 0.05, LCM3 *vs.* LCM6.1 ***p < 0.001, LCM3 *vs.* LCM4 **p < 0.01 (B) OB differentiation was assessed by ALP activity at day 7. Representative images illustrate ALP+-stained cultures. (C) ALP activity was quantified from cell lysates (day 7) normalized to the growth area (μM DIFMU per mm^2, mean ± SEM, n = 6). ***p < 0.001 (D) OB mineralization was detected by calcium deposits at day 14. Representative images show mineralized matrix visualised by ARS and von Kossa stains. (E) Mineralization was quantified from ARS-stained cultures by a cetylpyridinium chloride extraction method (day 14) shown as the concentration of ARS normalized to the growth area (ARS μM mm^{-2}, mean ± SEM, n = 5–6). ***p < 0.001.

In vivo evaluation of the bone response to LCM scaffolds

To evaluate the ability of the scaffolds to integrate into the calvarial bone defects, the three individual LCM scaffolds were inserted into the empty calvaria, and the scaffold structure and surrounding tissue were examined histologically (Fig. 3) after 12 weeks. In the sham (empty defect) control, a thin layer of fibrous tissue was observed over the entire defect but with an absence of bone or foreign materials. In contrast, when Vitoss (β-tricalcium-phosphate) was implanted, there were agglomerates and remnants of Vitoss bridging the defect area (visible in black). On high power field, it appears that Vitoss induced a dense fibrous tissue with some blood vessels and few inflammatory cells without evidence of new bone formation. Pink-stained areas are unspecific staining of Vitoss fragments or drilling remnants from the surgical procedure. Post implantation of 3D LCM scaffolds, no new bone formation was observed, but a significant difference in the structure of the scaffolds (scaffolds are blue in the bone sections). The LCM3 scaffold has an intact porous structure with loose connective tissue within the pores containing inflammatory cells and blood vessels. LCM4 also contains loose connective tissue, inflammatory cells and blood vessels, but is smaller and thinner than LCM3 despite having the exact same size at implantation. In contrast, LCM6.1 appears to be separated into 2 layers and contains less connective tissue, inflammatory cells and blood vessels within the pores compared with LCM3 and 4 scaffolds. Because there was no bone formation observed, no quantitative bone evaluation was done. Thus, the raw results are shown in histological sections.

Immunological responses to biomaterials

To assess the immunological responses to the biomaterials, both *in vivo* and *in vitro* responses were tested. Firstly, a high throughput *in vivo* model was used for rapid screening of immune reactions by implanting LCM scaffolds i.p. and measuring the cellular response and production of IL-1β, IL-2 and IL-4 (Fig. 4). In the negative sham control, less than 2×10^6 cells were observed and were predominantly peritoneal macrophages, with few eosinophils, lymphocytes, or neutrophils. In contrast, the positive Vitoss control had more than 4×10^6 cells which included a significant increase in macrophages, eosinophils and lymphocytes. All the LCM scaffolds generated minimal inflammatory responses that were similar to the sham control (Fig. 3A). The cytokine production mirrored these results with baseline values for IL-1β, IL-2 and IL-4 in the peritoneal fluid (Fig. 4B). In contrast, Vitoss significantly increased IL-1β and IL-4 compared to the sham controls in B6 and BALB/c mice, respectively.

To assess whether the LCMs induced inflammatory or fibrotic changes upon implantation, a subchronic model was used to examine histological sections for evidence of inflammation, foreign body giant cells (FBGCs) and fibrosis 12 weeks after implantation. The LCM scaffolds were compared to both the minimal inflammation in the sham control and the moderate response with FBGCs in response to Vitoss (Fig. 5). LCM3 and LCM4 induced mild inflammation without FBGCs compared to a more intense response observed with the LCM6.1 scaffolds. Fig. 5 illustrates that

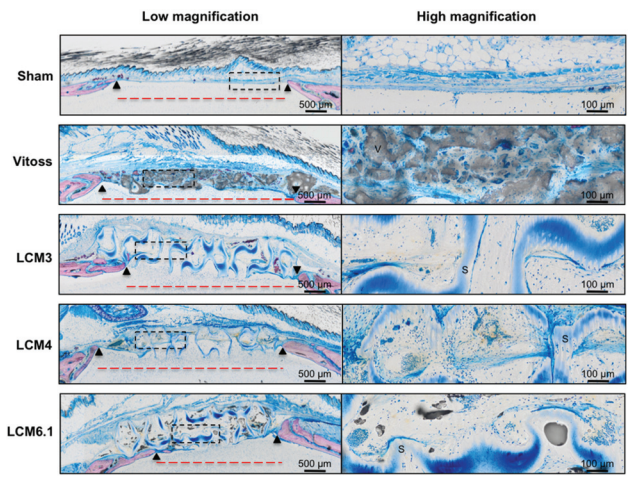

Fig. 3 *In vivo* evaluation of scaffolds in a calvarial defect model. Non-healing critical-sized calvarial defects were created in 12-week old female BALB/c mice by a 4 mm dental trephine. Treatment groups included sham control (empty defect), defects treated with Vitoss and the different LCM scaffolds (n = 5–6). Representative histological sections were prepared 12 weeks post-implantation. Formalin-fixed tissue was embedded in Technovit 7200 and sections (80–100 μm) were stained with Levai Laczko. The images are representative sections from individual mice and vary in size and shape. Photomicrographs are shown at low (left) and high (right) magnifications. Black triangles and red dotted lines indicate the bone defect; S: Scaffold; V: Vitoss.

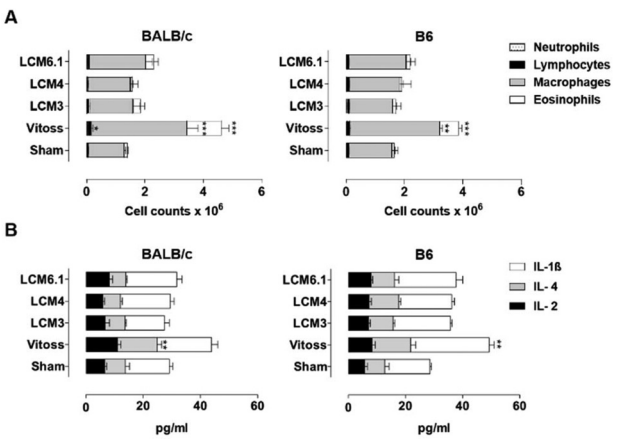

Fig. 4 Scaffold evaluation in a rapid high throughput mouse model. Female BALB/c and B6 mice were implanted i.p. with either LCM scaffolds, Vitoss, or no materials (sham). Seven days later, mice underwent peritoneal lavage. The lavage fluid was analyzed (A) for type and number of inflammatory cells (data are presented as mean cell counts ± SEM) and (B) for cytokine concentrations (data are presented as mean cytokine concentrations pg ml^{-1} ± SEM). These data are representative of two independent experiments (n = 5). *p < 0.05, **p < 0.01 and ***p < 0.001 is considered significant compared to sham.

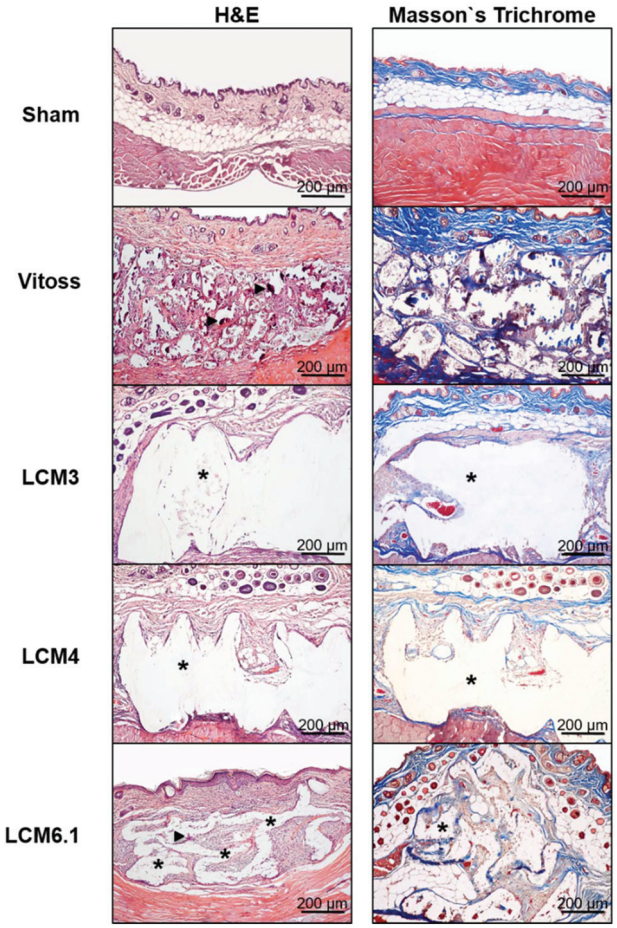

Fig. 5 Evaluation of scaffolds in a subchronic mouse model. Female BALB/c mice were implanted s.c. with either LCM scaffolds, Vitoss, or no materials (sham). At 12 weeks after implantation, skin from the implantation sites were incised and stained with H&E and Masson's Trichrome to evaluate wound healing and fibrosis. Photomicrographs of stained skin sections are shown at 10× and are representative of two independent experiments (n = 5). Arrows indicate FBGCs around the implant. *denotes degraded scaffolds.

Vitoss induced more collagen deposition compared with LCM3 and LCM4, which had collagen fibers around degraded scaffold filaments whereas LCM6.1 implantation induced even more collagen.

To determine whether the *in vivo* responses could be predicted by an *in vitro* assay, BALB/c and B6 splenocytes were incubated with LCM3, LCM4 and LCM6.1 scaffolds or Vitoss and then IL-1β, IL-2, IL-4 and IFNγ production and cell proliferation (Fig. 6) were measured. When the splenocytes were incubated with medium alone or in the presence of LCM scaffolds and Vitoss, cytokine secretion and cell proliferation were similar. However, in the presence of the mitogen, ConA, there is an expected increase in cell proliferation and cytokines for medium, Vitoss, LCM3, LCM4 and LCM6.1. There were minor differences in the magnitude of the responses between mouse strains, with the most evident difference being a higher BALB/c *vs.* B6 IL-4 response. Thus, the *in vitro* studies were predictive of the *in vivo* assay, though unable to provide information about the chronicity of inflammation and capacity to induce fibrosis.

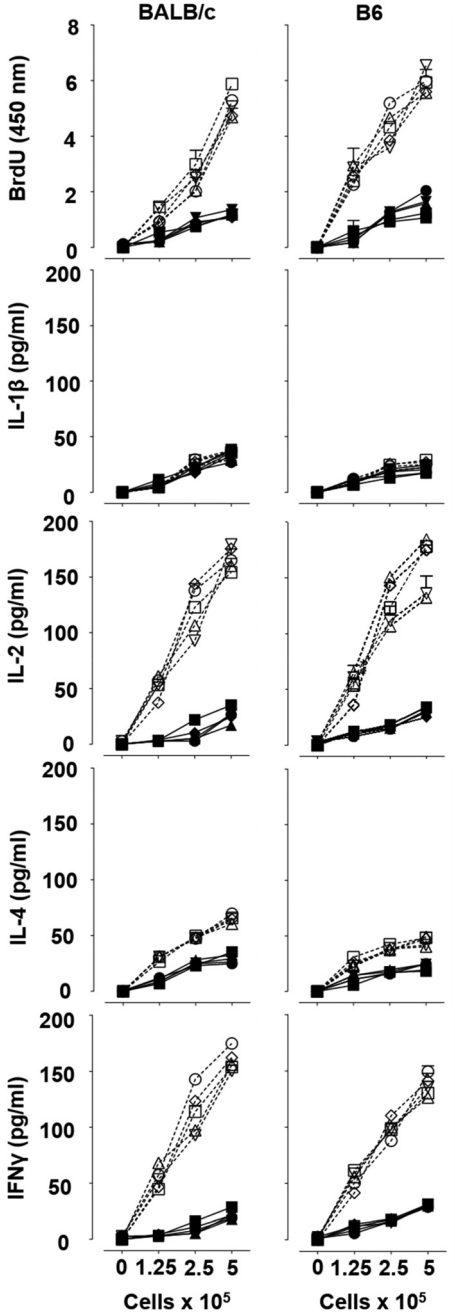

Fig. 6 Scaffold-induced *in vitro* cytokine production and cell proliferation. BALB/c and B6 splenocytes were cultured in the presence of LCM scaffolds or Vitoss. Cell proliferation, IL-1β, IL-2, IL-4 and IFNγ were measured upon incubation with either medium alone ●, ConA ○, Vitoss ■, Vitoss + ConA □, LCM3 ▲, LCM3 + ConA △, LCM4 ▼, LCM4 + ConA ▽, LCM6.1 ◆, LCM6.1 + ConA ◊ at 37 °C for 72 h. Proliferation results are presented as the mean of triplicate samples (BrdU (450 nm) absorbance ± SEM) in the BrdU assay and the mean of duplicate samples (pg ml^{-1} ± SEM) for cytokine concentration from two independent experiments. *p was considered significant at <0.05 for biomaterials *vs.* medium and biomaterials + ConA *vs.* ConA alone.

In vitro degradation and mechanical performance

In an attempt to determine whether physical properties of the scaffolds could correlate with the biological findings, the degradation and mechanical performance of the LCM scaffolds *in vitro* was explored. Fig. 7A shows the change in mass loss and pH of LCM3, LCM4 and LCM6.1 scaffolds throughout degradation in PBS at 37 °C for up to 90 days. Mass loss profiles for all scaffolds showed a two-stage linear increase with mass loss increased initially at a lower rate up to 28 days and followed by a more rapid rate until day 90. At the end of degradation experiment, LCM3 showed lower mass loss (*ca.* 24%) in comparison with LCM4 and LCM6.1 (*ca.* 30 and 36% respectively). The pH of the degradation medium, PBS, remained neutral for all specimens at approximately 7.4 ± 0.1 until the end of the degradation period at 90 days. The integrity of the scaffolds was traced during degradation by imaging at all time points using 4× magnification (Fig. 7B). LCM3 and 4 scaffolds remained intact until the end of the degradation study on day 90, whereas LCM6.1 collapsed at day 69.

Change in compressive modulus and strength of LCM3, 4 and 6.1 scaffolds *vs.* degradation time is shown in Fig. 8. Compressive moduli for LCM3, LCM4 and LCM6.1 scaffolds were *ca.* 0.18, 4.4 and 5.5 MPa, respectively before degradation. Compressive strengths at 20% strain for LCM4 and LCM6.1 scaffolds were more than 15 times higher than LCM3 (0.06 MPa). No changes were seen in both strength and modulus for all scaffolds over 85 days of degradation in PBS at 37 °C.

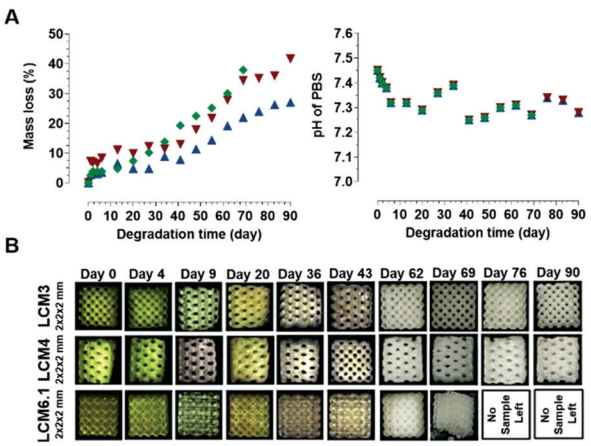

Fig. 7 Evaluation of copolymer degradation profile. (A) Change in mass loss and pH of degradation medium against time during degradation of LCM3 (blue triangle), LCM4 (red triangle) and LCM6.1 (green diamond) scaffolds in PBS at 37 °C. Scaffolds have dimensions of 2 mm^3. Error in mass loss measurement is less than 1% and contained within the symbol. (B) Integrity of the LCM scaffolds throughout *in vitro* degradation in PBS at 37 °C. Optical images were taken at all time points using 4× magnification. Scaffolds have dimensions of 2 mm^3. The change in the image colour was due to the change of the microscope camera during the study.

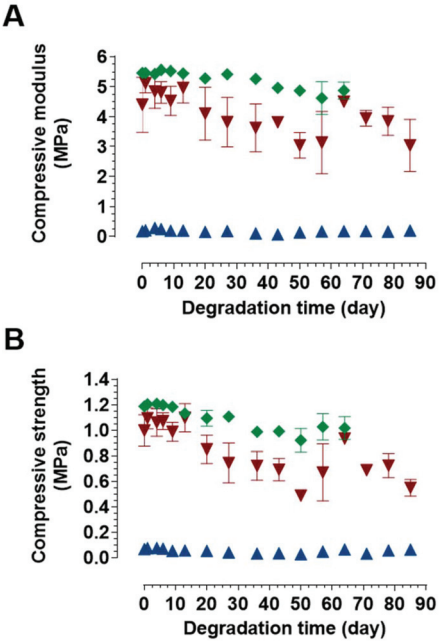

Fig. 8 Evaluation of mechanical properties. Retention of (A) compressive modulus and (B) compressive strength for LCM3 (blue triangle), LCM4 (red triangle) and LCM6.1 (green diamond) scaffolds *vs.* degradation time. Compressive strength was determined as the maximum stress at strain of 20%. The measurements were done 3 times and presented as MPa ± SD. Scaffolds have dimensions of 2 mm^3.

Discussion

The overall goal of this study was to evaluate the biological and physicochemical characteristics of novel customizable, biodegradable, biomimetic TPP-generated LCM copolymers as support scaffolds for bone fracture healing. We assessed the PLCL LCM3, LCM4 and LCM6.1 copolymers using *in vitro* and *in vivo* models and found an evident influence of the copolymer composition in all tests. The LCM6.1 scaffold reduced OC differentiation and OB proliferation compared with LCM3 and 4, while OB differentiation was similar for all scaffolds *in vitro.* LCM3 was more effective in the early stages of bone healing in the calvarial defect model than LCM4 and LCM6.1. In the *in vitro* splenocyte assays, all LCMs were immunologically inert. LCM3 and LCM4 scaffolds were well tolerated in the *in vivo* assays, though LCM6.1 induced more intense inflammation and fibrosis comparably in the subchronic mouse model. In *in vitro* degradation studies, LCM4 and LCM6.1 compared to LCM3 scaffolds had faster degradation rates and reduced mechanical retention. Our study demonstrates that TPP-generated LCM copolymer scaffolds, especially LCM3 with a lactide to caprolactone monomer ratio of 16 : 4 performs well in all tests. Overall, our results emphasize that polymer composition determines physical and biological properties and that these characteristics correlate. Our combined bone, immunological and physiochemical tests exemplify the benefit of a multidisciplinary strategy for preclinical evaluation of novel biomaterials for bone regeneration.

The innovative TPP microfabrication technology was used in manufacturing LCM scaffolds because of the ability to produce 3D polymeric microstructures of almost any desired complexity based on computer models and with a processing resolution of approximately 100 nm. The Schwarz P unit cell minimal surfaces have high stability utilizing less material[38] and more substantial fluid permeability in comparison to other pore structures geometries.[39] The Schwarz P structure is especially useful because it consists of channels and pores resembling cancellous bone which allows cell migration.

Scaffolds are structures designed to provide stability and to guide new bone formation. These materials were tested in a calvarial defect model in mice to determine the effect of LCM3, 4 and 6.1 scaffolds on bone repair. We found that the scaffolds alone did not induce new bone formation. Our findings support previous studies using a rat calvarial model[40] and a mandibular defect repair model in rabbits with PLGA scaffolds.[41] Moreover, we predicted this result because for normal bone healing, additional osteoinductive stimuli are necessary.[42] However, the scaffolds, compared to the sham controls, were associated with more early stage angiogenesis and tissue repair suggesting minimal bone repair in response to LCM3, 4 and 6.1 scaffolds.

There were two characteristics differentiating LCM3 and LCM4 from LCM6.1: after 12 weeks, LCM3 and 4 scaffolds were (1) thicker and (2) were associated with more cellular infiltrates than LCM6.1. A possible explanation for these observed differences may be due to degradation (thinning and fracturing of the scaffold of LCM6.1 in histological sections) and potential toxic degradation products leading to reduced cellular infiltration. These results are supported by the findings that there was accelerated degradation of LCM6.1 during *in vitro* degradation studies and the finding that LCM6.1 was associated with a different immune response compared to the other scaffolds. Taken together, data from *in vivo* and *in vitro* biological studies correlate with *in vitro* degradation studies.

While the LCM scaffolds did not induce bone formation in our calvaria model, it is important to note that Vitoss, a commercially available bone substitute material, did not induce new bone either. In support of this finding, Barbieri *et al.* implanted Vitoss in combination with Bioglass granules in a canine intraspinous implantation model and showed no bone formation.[43] In contrast, however, in both a mouse ectopic bone formation model and a rabbit critical defect femur model, Vitoss has been reported to induce bone formation.[44,45] There are several possible explanations for these contradicting data, including the animals, *e.g.*, mouse *vs.* rabbit and differences between the protocols. For example, one possibility is that bone healing rates differ between long bone and calvarial bone. Another possible explanation is that in the ectopic model, the skin provides a more reactive environment, *e.g.*, contains more inflammatory and other mediators promoting bone formation than in the calvarium. It is also possible that based on studies of clinical traumatic fractures, Vitoss works optimally because of the inflammatory environment in the injured site that provides mediators essential for bone repair.[44] Traumatic fractures differ substantially from the calvarial implantation site in this study, which was almost free of blood and thus, lacks circulating and local inflammatory mediators that might explain the lack of bone formation with Vitoss.

The *in vivo* bone repair studies indicated that early stages of repair occurred with differences between the LCM scaffolds tested. To further understand the LCM effects observed *in vivo*, we assessed the cellular response to the LCMs by investigating *in vitro* OB and OC responses. All the scaffolds increased OB proliferation compared with OM controls. However, only LCM3 resulted in a sustained increase in proliferation with comparably much less for LCM6.1. *In vitro* data show that LCM6.1 reduced OB proliferation and OC differentiation, whereas LCM6.1 > LCM4 > LCM3 increased OB mineralization while there was no influence by any scaffold on ALP activity at the time point measured. The difference in mineralization may be ascribed to the huge disparity in the compressive moduli of the scaffolds, LCM6.1 and 4 scaffolds are more than an order of magnitude higher than LCM3 (0.18 MPa). This finding supports the previous study on 3D hydrogel scaffolds with moduli ranged from 0.01 MPa to 0.3 MPa, which concluded that as the modulus increased to *ca.* 0.23 MPa, a significant increase in OB mineralization was observed.[46] These results also support a previous study with poly(L-lactic acid) that showed changes in OC differentiation.[47] Interestingly, the mechanical stiffness of the scaffolds (LCM6.1 > LCM4 > LCM3) appears to correlate with *in vitro* findings and supports previous studies showing that stiff- more than soft-substrates influenced OB differentiation and osteogenesis,[48–50] suggesting that increased mechanical stiffness modulates cell attachment, proliferation and differentiation. Remarkably, *in vitro* responses did not predict the outcome of *in vivo* bone repair which was also observed by other groups summarized in a review.[51] This disparity might be because the duration of the *in vivo* experiments (weeks) was longer than *in vitro* incubation periods (days), or because the LCMs are hydrophobic and could lead to the OBs taking longer to achieve confluence compared to cultures with osteogenic medium without scaffolds. Additional explanations may be related to the increased mass loss due to degradation of LCM4 and 6.1, compared with LCM3 (Fig. 7), resulting in increased degradation products influencing mineralization, or even the experimental conditions used. For example, *in vitro* differentiation is done with medium containing ascorbic acid and β-glycerophosphate to induce collagen production and promote differentiation to mature mineralizing OBs. However, there is no stimulation of osteogenesis *in vivo* because the scaffolds are not osteoinductive.

The early phase of bone healing is enhanced with an inflammatory microenvironment without chronic and aggressive inflammation, immune or allergic responses that may lead to reduced bone healing.[13] To assess immunogenicity and allergenicity of the scaffolds, we used *in vivo* and *in vitro* mouse models. We found that implantation of LCM3, LCM4 and LCM6.1 in the peritoneum (rapid throughput model) or under the skin (subchronic model) induced little inflam-

mation in the peritoneum and at the implantation sites, respectively. LCM6.1 scaffold induced more collagen fibers in the implantation site compared to LCM3 and LCM4, which is likely to be related to its faster degradation. This finding is consistent with previous studies showing that degradation products might cause undesired effects *via* local pH changes causing inflammation.[21] Cellular immune assays revealed that LCM3, LCM4 and LCM6.1 were unable to stimulate or inhibit splenocytes upon primary stimulation, indicating that these polymers are not toxic. Three immunological assays were performed to assess the immunogenicity and allergenicity of the scaffolds. The *in vitro* assays provide information on cytotoxicity, the i.p. response provides *in vivo* data on the inflammation and the cytokine milieu, while the s.c. reaction is long-term and provides information on the longevity of the inflammation and capacity to induce fibrosis. Our results support differences in inflammation caused by the LCMs in the calvarium experiments, with LCM3 and LCM4 but not LCM6.1 associated with inflammatory cell infiltrates at 12 weeks. While our i.p. and s.c. results demonstrate that these polymers are not highly immunologically reactive, they do appear to induce minimal inflammation in the bone, which is necessary for bone healing.[12,13,52,53] To ensure optimal bone repair, additional factors should be used in conjunction with the scaffolds. This is further supported with clinically relevant, Vitoss that is a successful bone graft material, because it contains bovine collagen type I that activates inflammation and OCs and OBs required for bone healing.[54,55]

The LCM scaffolds were designed for mechanical support and stability at the tissue site until new bone is fully matured and able to withstand mechanical load. Additionally, LCM scaffolds were intended to degrade and be resorbed at a controlled rate to allow *in vivo* formation of the new bone tissue.[56] Optimal degradation kinetics of scaffolds used for bone lesion healing remains unknown and requires further research. Ideally, the optimal polymer scaffold material should degrade and resorb at the same rate as tissue growth into the implant so it can be replaced with natural bone. PLA and PCL have been approved by the Food and Drug Administration and are suitable for cartilage and bone implants.[26] Importantly, their degradation and mechanical profiles can be tuned based on monomers ratio within their copolymer. They commonly require 1–3 years for complete degradation and their copolymers degrade faster than the homopolymers, depending on the LA to CL ratio.[26] An approach to achieve scaffolds with controlled degradation rates that fit specific biomedical application demands may be to use copolymers of two polymers with different degradation kinetics.[57]

It is advantageous to use an elastic and soft material to fabricate mechano-active scaffolds that can be used under cyclic mechanical strain. Jeong *et al.*[58,59] synthesized very flexible scaffolds based on copolymers of poly(glycolide-*co*-ε-caprolactone) and PLCL. Those scaffolds maintained a recovery of approximately 96% for two weeks under cyclic tensile strain (5 to 20%) in PBS.[59] Degradation in biological systems was validated by a non-biological *in vitro* assessment of degradation. LCM3 scaffolds revealed lower rate of mass loss compared with LCM4 and LCM6.1 (Fig. 7A), which was attributed to differences in LA/CL ratio between LCM3, 4 and 6.1 scaffold materials. LA/CL ratio for LCM3, LCM4 and LCM6.1 was 16/4, 18/2 and 9/1 respectively.[27] Degradation time, the required time for complete resorption, of PDLLA is approximately half of that for PCL.[60–62] Therefore, the increase in LA content would lead to a higher degradation rate. This explains the lower rate of mass loss for LCM3 in comparison with LCM4 and LCM6.1. However, LCM4 and LCM6.1 scaffolds contain the same LA/CL ratio, LCM6.1 degraded faster than LCM4. This was attributed to the difference in their initial molecular weight, *ca.* 1059 and 1822 g mol^{-1} for LCM6.1 and LCM4 respectively.[27] The difference in degradation rates among LCM scaffolds was also supported by optical images of the scaffold throughout the degradation period (Fig. 7B). LCM6.1 disintegrated into fragments by day 69, while LCM3 and 4 scaffolds remained intact until the end of the degradation study, which was ascribed to the fast degradation rate of LCM6.1 composition. The scaffolds lost *ca.* 20–35% on their initial weight throughout the degradation period, however, the pH of the degradation medium remained at neutral levels (7.4 ± 0.1) as a result of the buffering capability of PBS, gradual mass loss of the scaffolds and replacing the medium in a weekly basis.

Compressive properties of these scaffolds are mainly dependent on their compositions, specifically their LA/CL ratio, as all scaffolds have approximately similar porosity and pore sizes.[27] Elastic modulus for PCL is approximately five-fold lower than PDLLA.[60,61] Consequently, it was expected that mechanical properties of the scaffolds would decrease as the CL content increased within their copolymer. Bramfeldt *et al.*[63] demonstrated that rates of degradation and mechanical loss of PLCL copolymer increased gradually as the amount of LA changed from 0 to 70%.

Faster degradation means more inflammation and more tissue damage over the long-term. A good correlation was observed between *in vitro* and *in vivo* findings. LCM6.1 scaffolds showed faster degradation rate compared to LCM3 and 4 and consequently, revealed the least evidence for early stages of new bone formation. Such validated *in vitro* assays address the 3Rs research directed towards reducing animal experimentation with predictable *in vitro* assays and suggest that they are useful for pre-clinical assessment of bone repair biomaterials.

Conclusions

Our study focused on a novel biomimetic, biodegradable two-photon engineered PLCL repeating 3D Schwarz P minimal surface unit cell copolymer scaffold for the orthopedic surgeon to use for pain relief and to promote the repair of large non-union bone fractures. An integrated, multidisciplinary platform combining expertise in bone biology, immunology and materials science is a robust strategy which includes: (1) an *in vitro* evaluation of OBs and OCs and an *in vivo* mouse calvar-

ial defect model, (2) *in vitro* and *in vivo* evaluation of inflammatory, immune and allergic reactions to biomaterials, and (3) *in vitro* degradation and mechanical compression and strength studies. Our results indicate that these copolymers will perform well in the clinic for bone repair because they can be tailor-made for exact fit in large bone lesions, the scaffolds with the optimal copolymer composition are immunologically compatible, allow for normal OB and OC function and promote bone healing. Moreover, these scaffolds have mechanical properties designed in consultation with surgeons to have at least 20% recoverable compression for fitting them into bone fracture sites. The degradation studies *in vitro* agree with *in vivo* observations and indicate that they degrade in a suitable period which is sufficient for physiological bone replacement. This study illustrates an important new biomaterial with a strategy for pre-clinical evaluation of biomaterials developed for bone repair.

Conflicts of interest

There are no conflicts to declare.

Acknowledgements

The authors wish to thank our colleagues at the Institute for Bioprocessing and Analytical Measurement Techniques for providing the samples as part of the EC FP7 InnovaBone project and thank Drs Serena Best and Sahar Kazemi for the critical reading of the manuscript. This research project has received funding from the European Union's Seventh Framework Programme (FP7/2007–2013) under grant agreement no. 263363. This work was supported by the Engineering and Physical Sciences Research Council [grant number EP/K029592/1]; and the EPSRC Centre for Innovative Manufacturing in Medical Devices (MeDe Innovation).

References

1 E. Garcia-Gareta, M. J. Coathup and G. W. Blunn, *Bone*, 2015, **81**, 112–121.
2 R. Yunus Basha, T. S. Sampath Kumar and M. Doble, *Mater. Sci. Eng., C*, 2015, **57**, 452–463.
3 I. Dumic-Cule, M. Pecina, M. Jelic, M. Jankolija, I. Popek, L. Grgurevic and S. Vukicevic, *Int. Orthop.*, 2015, **39**, 1005–1011.
4 M. Bumbasirevic, M. Stevanovic, V. Bumbasirevic, A. Lesic and H. D. Atkinson, *Int. Orthop.*, 2014, **38**, 1277–1282.
5 J. A. Goulet, L. E. Senunas, G. L. DeSilva and M. L. Greenfield, *Clin. Orthop. Relat. Res.*, 1997, 76–81.
6 Z. S. Ai-Aql, A. S. Alagl, D. T. Graves, L. C. Gerstenfeld and T. A. Einhorn, *J. Dent. Res.*, 2008, **87**, 107–118.
7 E. Tsiridis, N. Upadhyay and P. Giannoudis, *Injury*, 2007, **38**, S11–S25.
8 K. Merritt and J. J. Rodrigo, *Clin. Orthop. Relat. Res.*, 1996, **326**, 71–79.
9 L. C. Gerstenfeld, D. M. Cullinane, G. L. Barnes, D. T. Graves and T. A. Einhorn, *J. Cell. Biochem.*, 2003, **88**, 873–884.
10 X. Li, R. J. Quigg, J. Zhou, J. T. Ryaby and H. Wang, *J. Cell. Biochem.*, 2005, **95**, 189–205.
11 C. N. Medine, F. Khan, S. Pernagallo, R. Zhang, O. Tura, M. Bradley and D. C. Hay, in *Biomaterials and stem cells in regenerative medicine*, ed. M. Ramalingam, S. Ramakrishna and S. Best, 2012, pp. 1–30.
12 H. C. Pape, R. Marcucio, C. Humphrey, C. Colnot, M. Knobe and E. J. Harvey, *J. Orthop. Traumatol.*, 2010, **24**, 522–525.
13 O. Bastian, J. Pillay, J. Alblas, L. Leenen, L. Koenderman and T. Blokhuis, *J. Leukocyte Biol.*, 2011, **89**, 669–673.
14 D. G. Tamay, T. Dursun Usal, A. S. Alagoz, D. Yucel, N. Hasirci and V. Hasirci, *Front. Bioeng. Biotechnol.*, 2019, **7**, 1–22.
15 D. W. Hutmacher, *Biomaterials*, 2000, **21**, 2529–2543.
16 B. Dhandayuthapani, Y. Yoshida, T. Maekawa and D. S. Kumar, *Int. J. Polym. Sci.*, 2011, **2011**, 1–19.
17 P. A. Gunatillake and R. Adhikari, *Eur. Cells Mater.*, 2003, **5**, 1–16.
18 B. D. Ulery, L. S. Nair and C. T. Laurencin, *J. Polym. Sci., Part B: Polym. Phys.*, 2011, **49**, 832–864.
19 R. Sartoneva, K. Kuismanen, M. Juntunen, S. Karjalainen, M. Hannula, L. Kyllönen, J. Hyttinen, H. Huhtala, K. Paakinaho and S. Miettinen, *R. Soc. Open Sci.*, 2018, **5**, 180811–180811.
20 K. K. Moncal, D. N. Heo, K. P. Godzik, D. M. Sosnoski, O. D. Mrowczynski, E. Rizk, V. Ozbolat, S. M. Tucker, E. M. Gerhard, M. Dey, G. S. Lewis, J. Yang and I. T. Ozbolat, *J. Mater. Res.*, 2018, **33**, 1972–1986.
21 S. Lyu and D. Untereker, *Int. J. Mol. Sci.*, 2009, **10**, 4033–4065.
22 Taylor and Francis Group, *Biomaterial fabrication and processing handbook*, CRC Press, 2008.
23 O. Al-Ketan, R. Rezgui, R. Rowshan, H. Du, N. X. Fang and R. K. Abu Al-Rub, *Adv. Eng. Mater.*, 2018, **20**, 1800029.
24 M. Malinauskas, P. Danilevicius and S. Juodkazis, *Opt. Express*, 2011, **19**, 5602–5610.
25 A. P. Moreno Madrid, S. M. Vrech, M. A. Sanchez and A. P. Rodriguez, *Mater. Sci. Eng., C*, 2019, **100**, 631–644.
26 J. Holmbom, A. Sodergard, E. Ekholm, M. Martson, A. Kuusilehto, P. Saukko and R. Penttinen, *J. Biomed. Mater. Res., Part A*, 2005, **75**, 308–315.
27 R. M. Felfel, L. Poocza, M. Gimeno-Fabra, T. Milde, G. Hildebrand, I. Ahmed, C. Scotchford, V. Sottile, D. M. Grant and K. Liefeith, *Biomed. Mater.*, 2016, **11**, 1–14.
28 R. M. Felfel, D. Gupta, A. Z. Zabidi, A. Prosser, C. A. Scotchford, V. Sottile and D. M. Grant, *Mater. Des.*, 2018, **160**, 455–467.
29 R. M. Felfel, L. Poocza, M. Gimeno-Fabra, T. Milde, G. Hildebrand, I. Ahmed, C. Scotchford, V. Sottile, D. M. Grant and K. Liefeith, *Biomed. Mater.*, 2016, **11**, 015011.

30 N. Takahashi, T. Akatsu, N. Udagawa, T. Sasaki, A. Yamaguchi, J. M. Moseley, T. J. Martin and T. Suda, *Endocrinology*, 1988, **123**, 2600–2602.
31 A. D. Bakker and J. Klein-Nulend, in *Bone Research Protocols*, ed. M. Helfrich and S. Ralston, Humana Press, 2012, vol. 816, pp. 19–29.
32 F. Meyer, J. Wardale, S. Best, R. Cameron, N. Rushton and R. Brooks, *J. Orthop. Res.*, 2012, **30**, 864–871.
33 K. Changi, B. Bosnjak, C. Gonzalez-Obeso, R. Kluger, J. C. Rodriguez-Cabello, O. Hoffmann and M. M. Epstein, *J. Biomed. Mater. Res., Part A*, 2018, **106**, 924–934.
34 K. S. Jones, *Semin. Immunol.*, 2008, **20**, 130–136.
35 D. M. Higgins, R. J. Basaraba, A. C. Hohnbaum, E. J. Lee, D. W. Grainger and M. Gonzalez-Juarrero, *Am. J. Pathol.*, 2009, **175**, 161–170.
36 ISO, *BS EN ISO 10993-13: Biological evaluation of medical devices. Identification and quantification of degradation products from polymeric medical devices*, 2010.
37 Y. Jung, S. H. Kim, Y. H. Kim and S. H. Kim, *Biomed. Mater.*, 2009, **4**, 1–7.
38 S. Torquato, S. Hyun and A. Donev, *Phys. Rev. Lett.*, 2002, **89**, 1–4.
39 Y. Jung and S. Torquato, *Phys. Rev. E: Stat., Nonlinear, Soft Matter Phys.*, 2005, **72**, 1–8.
40 C. Zong, D. T. Xue, W. J. Yuan, W. Wang, D. Shen, X. M. Tong, D. Y. Shi, L. Y. Liu, Q. A. Zheng, C. Y. Gao and J. F. Wang, *Eur. Cells Mater.*, 2010, **20**, 109–120.
41 T. B. Ren, J. Ren, X. Z. Jia and K. F. Pan, *J. Biomed. Mater. Res., Part A*, 2005, **74**, 562–569.
42 A. Cipitria, J. C. Reichert, D. R. Epari, S. Saifzadeh, A. Berner, H. Schell, M. Mehta, M. A. Schuetz, G. N. Duda and D. W. Hutmacher, *Biomaterials*, 2013, **34**, 9960–9968.
43 D. Barbieri, H. Yuan, A. S. Ismailoglu and J. D. de Bruijn, *Tissue Eng., Part A*, 2017, **23**, 1310–1320.
44 S. J. Roberts, L. Geris, G. Kerckhofs, E. Desmet, J. Schrooten and F. P. Luyten, *Biomaterials*, 2011, **32**, 4393–4405.
45 W. R. Walsh, R. A. Oliver, C. Christou, V. Lovric, E. R. Walsh, G. R. Prado and T. Haider, *PLoS One*, 2017, **12**, 1–21.
46 K. Chatterjee, S. Lin-Gibson, W. E. Wallace, S. H. Parekh, Y. J. Lee, M. T. Cicerone, M. F. Young and C. G. Simon, *Biomaterials*, 2010, **31**, 5051–5062.
47 G. L. Jones, A. Motta, M. J. Marshall, A. J. El Haj and S. H. Cartmell, *Biomaterials*, 2009, **30**, 5376–5384.
48 A. S. Mao, J. W. Shin and D. J. Mooney, *Biomaterials*, 2016, **98**, 184–191.
49 Y. R. Shih, K. F. Tseng, H. Y. Lai, C. H. Lin and O. K. Lee, *J. Bone Miner. Res.*, 2011, **26**, 730–738.
50 N. D. Evans, C. Minelli, E. Gentleman, V. LaPointe, S. N. Patankar, M. Kallivretaki, X. Chen, C. J. Roberts and M. M. Stevens, *Eur. Cells Mater.*, 2009, **18**, 1–14.
51 G. Hulsart-Billstrom, J. I. Dawson, S. Hofmann, R. Muller, M. J. Stoddart, M. Alini, H. Redl, A. El Haj, R. Brown, V. Salih, J. Hilborn, S. Larsson and R. O. C. Oreffo, *Eur. Cells Mater.*, 2016, **31**, 312–322.
52 I. H. Kalfas, *Neurosurg Focus*, 2001, **10**, 1–4.
53 K. Schmidt-Bleek, H. Schell, N. Schulz, P. Hoff, C. Perka, F. Buttgereit, H. D. Volk, J. Lienau and G. N. Duda, *Cell Tissue Res.*, 2012, **347**, 567–573.
54 M. P. Bostrom and D. A. Seigerman, *HSS J.*, 2005, **1**, 9–18.
55 C. Van Hoff, J. B. Samora, M. J. Griesser, M. K. Crist, T. J. Scharschmidt and J. L. Mayerson, *Am. J. Orthop.*, 2012, **41**, 20–23.
56 J. Henkel, M. A. Woodruff, D. R. Epari, R. Steck, V. Glatt, I. C. Dickinson, P. F. Choong, M. A. Schuetz and D. W. Hutmacher, *Bone Res.*, 2013, **1**, 216–248.
57 V. Guarino, F. Causa, P. Taddei, M. di Foggia, G. Ciapetti, D. Martini, C. Fagnano, N. Baldini and L. Ambrosio, *Biomaterials*, 2008, **29**, 3662–3670.
58 S. I. Jeong, J. H. Kwon, J. I. Lim, S. W. Cho, Y. Jung, W. J. Sung, S. H. Kim, Y. H. Kim, Y. M. Lee, B. S. Kim, C. Y. Choi and S. J. Kim, *Biomaterials*, 2005, **26**, 1405–1411.
59 S. I. Jeong, B. S. Kim, Y. M. Lee, K. J. Ihn, S. H. Kim and Y. H. Kim, *Biomacromolecules*, 2004, **5**, 1303–1309.
60 P. B. Maurus and C. C. Kaeding, *Oper. Tech. Sports Med.*, 2004, **12**, 158–160.
61 J. C. Middleton and A. J. Tipton, *Biomaterials*, 2000, **21**, 2335–2346.
62 M. A. Woodruff and D. W. Hutmacher, *Prog. Polym. Sci.*, 2010, **35**, 1217–1256.
63 H. Bramfeldt, P. Sarazin and P. Vermette, *J. Biomed. Mater. Res., Part A*, 2007, **83**, 503–511.